

Structure and energetics of mixed ^4He - ^3He drops

M. Barranco and M. Pi

Departament d'Estructura i Constituents de la Matèria, Facultat de Física, Universitat de Barcelona, E-08028 Barcelona, Spain

S. M. Gatica and E. S. Hernández

Departamento de Física, Facultad de Ciencias Exactas y Naturales, Universidad de Buenos Aires, 1428 Buenos Aires, Argentina

J. Navarro

IFIC (Centro Mixto CSIC Universitat de València), Facultat de Física, E-46100 Burjassot, València, Spain

(Received 8 April 1997)

Using a finite-range density functional, we have investigated the energetics and structural features of mixed helium clusters. The possibility of doping the cluster with a molecule of sulfur hexafluoride is also considered. It is seen that the repulsion introduced by the impurity strongly modifies the properties of the smallest drops. Although only a qualitative comparison is possible, the gross features displayed by our calculations are in agreement with recent experimental findings. [S0163-1829(97)02438-7]

I. INTRODUCTION

Despite its considerable difficulty, the study of liquid helium drops has been a subject of great theoretical and experimental interest.^{1,2} Up to very recently, the major limitations have been the experimental impossibility of selecting and identifying clusters of a given size, or at least, within a narrow size distribution, and the fact that most experiments were carried out on $^4\text{He}_N$ clusters. These issues prevented a sensible comparison with available calculations and rendered academic some of the published theoretical studies, discouraging further investigations within the reach of theorists.

The situation is rapidly improving. Better scattering deflection methods are now able to size-select large helium clusters,³ and molecular beam diffraction from a transmission grating seems able to do the same for small van der Waals clusters.⁴ The drops can then be analyzed and the data compared with theory, a possibility that not long ago was unthinkable.

A field of emerging interest nowadays, is the analysis of pure and mixed ^3He - ^4He clusters with doping atoms or molecules. The best studied systems are ^4He clusters doped with atomic impurities and SF_6 molecules (see Refs. 5–11, and references therein). The major outcomes of that body of work are to have established the location of the impurity in the bulk of the drop, and the fact that due to their low temperature, which is around 0.4 K for ^4He ,⁶ liquid drops provide useful ultracold matrices well suited for high resolution molecular spectroscopy. That temperature is even lower in the case of ^3He , some 0.15 K,¹² in good agreement with the predictions of Ref. 13.

Concerning pure ^3He drops, the first systematic study of their ground state properties was carried out by Pandharipande and co-workers using a variational Monte Carlo (VMC) technique,¹⁴ and by Stringari and Treiner within a local, zero-range energy-density-functional (LDF) approximation.¹⁵ There are also two recent systematic calculations which make use of nonlocal, finite-range density functionals (FRDF) built so as to reproduce a large number

of properties of the homogeneous and inhomogeneous liquid.^{16,17} Within LDF, a random-phase approximation calculation of the collective spectrum of close shell ^3He drops is also available.¹⁸ FRDF results for open-shell ^3He droplets has also been reported.¹⁹ As we have indicated, the theoretical effort have been hampered so far by the lack of experimental results on ^3He drops on one hand, and of a full microscopic theory, in contradistinction with the ^4He case, on the other hand.

In this work we present an investigation of $^3\text{He}_N$ - $^4\text{He}_M$ and $^3\text{He}_N$ - $^4\text{He}_M$ + SF_6 drops, systems for which experimental results are becoming available.¹² Previous calculations were carried out for one ^3He impurity in ^4He drops.^{20,21} In particular, in Ref. 20 a zero-range density functional was employed to describe both the ^4He drop and the ^3He - ^4He interaction. However, it has been recognized that functionals of this kind are not accurate enough to deal with finite-size effects, especially when the drop hosts an impurity that provokes a strong density compression. These drawbacks are removed by the inclusion of finite range interaction terms in the density functional; for this sake, in the present approach we introduce a FRDF adequate to describe properties of helium mixtures, which is presented in Sec. II, together with the method of calculation. The results for ^4He drops doped with one ^3He atom are presented in Sec. III, and IV for mixed drops. Finally, we draw our conclusions in Sec. V.

II. THE FINITE-RANGE DENSITY FUNCTIONAL FOR MIXED HELIUM DROPS

We consider that the total energy of a liquid-helium mixture can be expressed as a density functional of their particle densities ρ_3, ρ_4 , and of the kinetic energy density τ_3 of ^3He :

$$E[\rho_3, \tau_3, \rho_4] = \int d\vec{r} \{ \mathcal{E}_4[\rho_3, \rho_4] + \mathcal{E}_3[\rho_3, \tau_3, \rho_4] + \mathcal{E}_{34}[\rho_3, \rho_4] \}, \quad (1)$$

where

TABLE I. Parameters of the density functional.

b_4 (K Å ³)	c_4' (K Å ⁶)	c_4'' (K Å ⁹)	b_3 (K Å ³)	$c_3'+c_3''$ (K Å ^{3+γ₃})	c_3'' (K Å ^{3+γ₃})	$γ_3$
-718.99	-2.41186×10 ⁴	1.85850×10 ⁶	-684.676	1.55379×10 ⁶	-3.5×10 ⁴	2.1251
b_{34} (K Å ³)	c_{34} (K Å ^{3+γ₃₄})	$γ_{34}$	$α_s$ (K ⁻¹ Å ³)	$ρ_{0s}$ (Å ⁻³)	$ρ_{3c}$ (Å ⁻³)	$ρ_{4c}$ (Å ⁻³)
-662.8	4.5×10 ⁶	2.6565	54.31	0.04	0.0406	0.062
$ε_{LJ}$ (K)	h_3 (Å)	h_4 (Å)	h_{34} (Å)	$σ_3$ (Å)	$σ_4$ (Å)	$σ_{34}$ (Å)
10.22	2.11311	2.190323	2.176374	2.46	2.556	2.5455

$$\begin{aligned}
\mathcal{E}_4[\rho_3, \rho_4] = & \frac{\hbar^2}{2m_4} (\nabla \sqrt{\rho_4(\vec{r})})^2 + \frac{1}{2} \int d\vec{r}' \rho_4(\vec{r}) V_4(|\vec{r}-\vec{r}'|) \\
& \times \rho_4(\vec{r}') + \frac{1}{2} c_4' \rho_4(\vec{r}) [\bar{\rho}_3(\vec{r}) + \bar{\rho}_4(\vec{r})]^2 \\
& + \frac{1}{3} c_4'' \rho_4(\vec{r}) [\bar{\rho}_3(\vec{r}) + \bar{\rho}_4(\vec{r})]^3 \\
& - \frac{\hbar^2}{4m_4} \alpha_s \int d\vec{r}' F(|\vec{r}-\vec{r}'|) \left[1 - \frac{\tilde{\rho}_4(\vec{r}')}{\rho_{0s}} \right] \\
& \times \nabla \rho_4(\vec{r}) \cdot \nabla \rho_4(\vec{r}') \left[1 - \frac{\tilde{\rho}_4(\vec{r}')}{\rho_{0s}} \right], \quad (2)
\end{aligned}$$

$$\begin{aligned}
\mathcal{E}_3[\rho_3, \tau_3, \rho_4] = & \frac{\hbar^2}{2m_3^*} \tau_3 + \frac{1}{2} \int d\vec{r}' \rho_3(\vec{r}) V_3(|\vec{r}-\vec{r}'|) \rho_3(\vec{r}') \\
& + \frac{1}{2} c_3' \rho_3^2(\vec{r}) [\bar{\rho}_3(\vec{r}) + \bar{\rho}_4(\vec{r})]^{\gamma_3} \\
& + \frac{1}{2} c_3'' \rho_3^2(\vec{r}) \bar{\rho}_3(\vec{r})^{\gamma_3}, \quad (3)
\end{aligned}$$

$$\begin{aligned}
\mathcal{E}_{34}[\rho_3, \rho_4] = & \int d\vec{r}' \rho_3(\vec{r}) V_{34}(|\vec{r}-\vec{r}'|) \rho_4(\vec{r}') \\
& + c_{34} \rho_3(\vec{r}) \rho_4(\vec{r}) [\bar{\rho}_3(\vec{r}) + \bar{\rho}_4(\vec{r})]^{\gamma_{34}}. \quad (4)
\end{aligned}$$

In these expressions, $\bar{\rho}_i(\vec{r})$ for $i=3,4$ is an averaged density given by

$$\bar{\rho}_i(\vec{r}) = \int d\vec{r}' \rho_i(\vec{r}') w_i(|\vec{r}-\vec{r}'|), \quad (5)$$

where

$$\begin{aligned}
w_i(|\vec{r}|) = & \frac{3}{4\pi h_i^3} \text{ if } |\vec{r}| < h_i, \\
& 0 \text{ otherwise.} \quad (6)
\end{aligned}$$

In addition, $V_i(|\vec{r}-\vec{r}'|)$ ($i=3, 4$ or 34) is a finite range interaction consisting of a Lennard-Jones (LJ) potential with truncated core

$$\begin{aligned}
V_i(r) = & 4\epsilon_{LJ} \left[\left(\frac{\sigma_i}{r} \right)^{12} - \left(\frac{\sigma_i}{r} \right)^6 \right] \text{ if } r \geq h_i, \\
& 0 \text{ otherwise} \quad (7)
\end{aligned}$$

and $F(|\vec{r}-\vec{r}'|)$ is a Gaussian kernel with dispersion l equal to unity:

$$F(r) = \frac{1}{\pi^{3/2} l^3} e^{-r^2/l^2}, \quad (8)$$

which is also used to define the other averaged density entering \mathcal{E}_4 :

$$\tilde{\rho}_4(\vec{r}) = \int d\vec{r}' \rho_4(\vec{r}') F(|\vec{r}-\vec{r}'|). \quad (9)$$

\mathcal{E}_4 reduces to the Orsay-Trento (OT) density functional²² setting ρ_3 to zero. \mathcal{E}_3 and \mathcal{E}_{34} are finite-range generalizations of the density functional introduced in Ref. 23 (see also Ref. 24), from where we have also taken the parametrization of the effective mass of ³He, which was selected so as to fit the experimental data presented in Ref. 25:

$$\frac{\hbar^2}{2m_3^*} = \frac{\hbar^2}{2m_3} \left(1 - \frac{\bar{\rho}_3}{\rho_{3c}} - \frac{\bar{\rho}_4}{\rho_{4c}} \right)^2. \quad (10)$$

The use of the OT functional makes it necessary to readjust the value of some of the original parameters entering \mathcal{E}_3 and \mathcal{E}_{34} . We have also changed σ_3 from its standard value to exactly reproduce the experimental surface tension of liquid ³He that otherwise would have been some 10% higher. The size of the vanishing LJ cores h_i in Eq. (7) has been fixed as indicated in Ref. 24 and the remaining parameters so as to get the best possible fit to the maximum solubility x_M of ³He into liquid ⁴He, the excess volume coefficient and the osmotic pressure at various pressures between 0 and 20 atm for the liquid helium mixtures, together with the surface tension of the ³He-⁴He interface at zero temperature and saturation pressure. The set of coefficients of the whole density func-

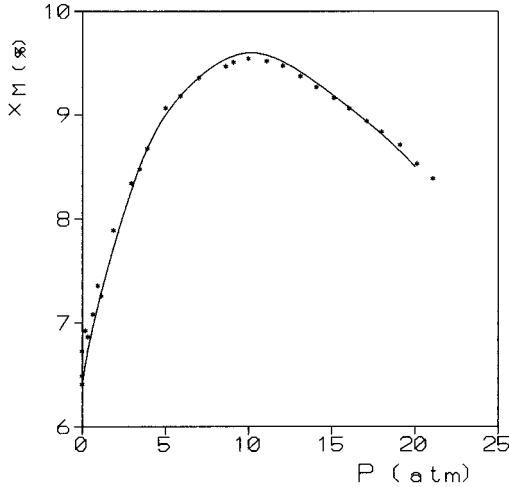


FIG. 1. The maximum solubility of ^3He into liquid ^4He in % as a function of pressure in atm. The experimental points have been taken from Ref. 32.

tional (1) is given in Table I. In this table, the quantity b_i is the volume integral of the corresponding LJ potential²²

$$b_i = \int d\vec{r} V_i(|\vec{r}|). \quad (11)$$

Altogether, we have achieved an accurate description of the above mentioned thermodynamical properties of the mixture and its interfaces. For the sake of an example, we show in Fig. 1 the maximum solubility, and in Fig. 2 the surface tension of the ^3He - ^4He interface as a function of pressure. These two magnitudes were only roughly described previously.²³

For a cluster made of given number of atoms of each type N_4 and N_3 , their structure and energetics result from the solution of the coupled Hartree²⁶ and Hartree-Fock²⁷ equations corresponding to each isotope, easily deduced from Eq. (1).^{22,27} In the case of ^3He , the particle and kinetic energy densities are obtained from the single particle wave functions $\phi_j(\vec{r})$

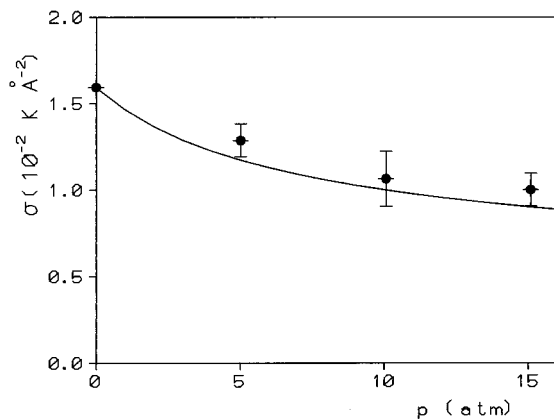


FIG. 2. The surface tension of the ^3He - ^4He interface as a function of pressure in atm together with experimental data from Ref. 33.

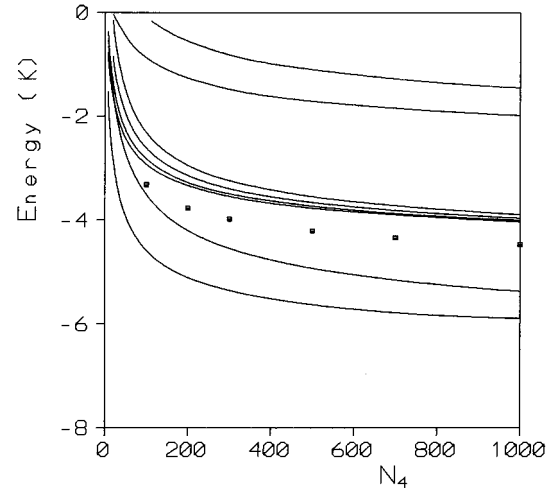


FIG. 3. From bottom to top the curves respectively represent, in K, the chemical potential μ_4 , the energy per particle E_4/N_4 , the single particle energies of states $1s$, $1p$, $1d$, $1f$, $2s$, and $3s$ of one ^3He atom, as functions of N in $^4\text{He}_N$ clusters. The squares correspond to the $1s$ energies reported in Ref. 20.

$$\rho_3(\vec{r}) = \sum_{j=1}^{N_3} |\phi_j(\vec{r})|^2 = \sum_{nlm} \left| \frac{R_{nl}(r)}{r} Y_{lm}(\hat{r}) \right|^2, \quad (12)$$

$$\tau_3(\vec{r}) = \sum_{j=1}^{N_3} |\nabla \phi_j(\vec{r})|^2. \quad (13)$$

The diagonal part of the center-of-mass correction²⁷ has been taken into account making the following substitutions in the kinetic energy terms:

$$\frac{\hbar^2}{2m_3} \rightarrow \frac{\hbar^2}{2m_3} \left(1 - \frac{1}{N_3 + (m_4/m_3)N_4} \right), \quad (14)$$

$$\frac{\hbar^2}{2m_4} \rightarrow \frac{\hbar^2}{2m_4} \left(1 - \frac{1}{N_4 + (m_3/m_4)N_3} \right). \quad (15)$$

As in previous investigations concerning ^4He drops,^{7,8,20} when we consider the possibility of the cluster being doped with sulfur hexafluoride, the molecule is regarded as an object with infinite mass located at the coordinate origin and providing an external field to all helium atoms. The potential for the spherically averaged SF_6 -He potential, which should be added to either single particle (SP) mean field, is taken from Ref. 28.

III. SYSTEMATICS OF A SINGLE ^3He ATOM IN PURE AND DOPED ^4He DROPLETS

As we add one single ^3He atom to a given ^4He cluster, a variety of energetic features can be investigated as a function of the number of particles in the droplet N_4 . After self-consistently determining the energy per particle E_4/N_4 and the chemical potential μ_4 of the ^4He atoms, the peculiarities of the ^3He spectrum depend upon N_4 as visualized in Figs. 3–6.

In Fig. 3 we display the single particle energies of the four lowest lying levels of this spectrum, as well as those of the

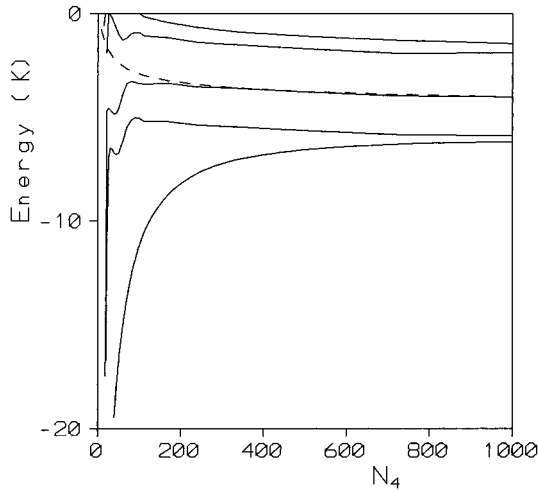


FIG. 4. From bottom to top the curves respectively represent, in K, the chemical potential μ_4 , the energy per particle E_4/N_4 , the SP energies of states $1s$, $2s$ and $3s$ of one ${}^3\text{He}$ atom, as functions of the N in doped ${}^4\text{He}_N+\text{SF}_6$ clusters. The dashed line corresponds to the $1s$ energy of the ${}^3\text{He}$ atom in the pure droplets.

next two higher s states, as functions of N_4 . The squares indicate the $1s$ energies presented in Ref. 20. For completeness, we plot as well the energy per particle and chemical potential of the host cluster. We can realize that the present FRDF is more repulsive on ${}^3\text{He}$ atoms than the zero-range one employed in Ref. 20; this feature also shows up when we fit the trend of ε_{1s} to a mass formula of the type

$$\varepsilon_{1s} = \varepsilon_0 + \frac{C}{N_4^{1/3}}, \quad (16)$$

with $\varepsilon_0 = -4.81$ K and $C = 8.44$ K.²⁹ These parameters have been obtained including drops as large as $N_4 = 10^4$. Representing ε_0 the chemical potential of the ${}^3\text{He}$ atom on the surface of liquid ${}^4\text{He}$ at zero pressure, we observe that the

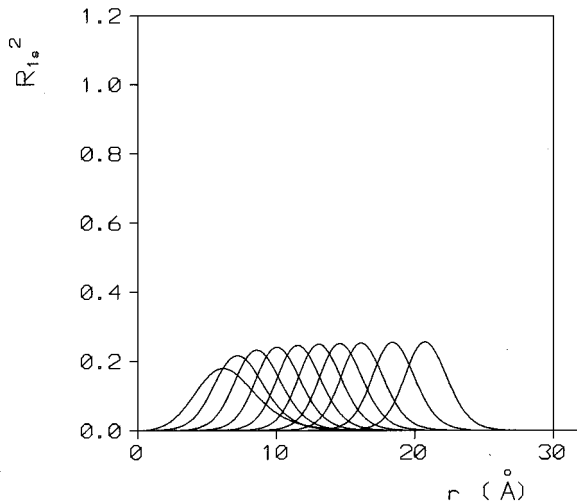


FIG. 5. The radial probability density $|R_{1s}(r)|^2$ of the ${}^3\text{He}$ atom in ${}^4\text{He}_N$ as a function of the distance to the center of the droplet for, from left to right, $N_4 = 8, 20, 40, 70, 112, 168, 240, 330, 500,$ and 728 .

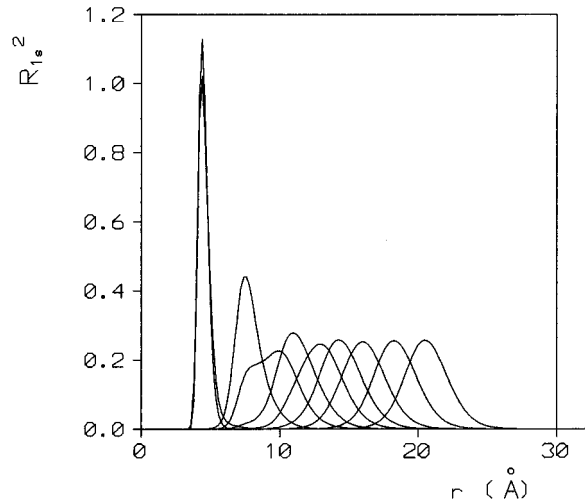


FIG. 6. Same as Fig. 5 for ${}^4\text{He}_N+\text{SF}_6$.

current value is reasonably close to the energy of the Andreev state, namely, $\varepsilon_0 = (-5.00 \pm 0.03)$ K.³⁰ Notice that in Ref. 20, the corresponding values are $\varepsilon_0 = -5.44$ K and $C = 9.8$ K, and that the variational Monte Carlo calculation of²¹ yields $\varepsilon_0 \sim -4.90$ K. It is also apparent from this figure that as the size of the ${}^4\text{He}$ cluster increases, the spectrum of the ${}^3\text{He}$ atom becomes rather independent of the orbital quantum number. The rate of degeneracy is higher for states with radial quantum number equal to unity; this tendency can be confirmed examining the corresponding wave functions and their mean square radius, which become almost coincident when the drop contains a few hundreds of particles. This degeneracy reflects the physical fact that in the limit of a large drop, the surface ${}^3\text{He}$ states would no longer be adequately characterized by an angular momentum quantum number, but rather by a linear momentum parallel to the free surface, whose multipolar decomposition will in practice need a large superposition of partial waves.

An interesting property, already observed by Dalfovo,²⁰ is that as the number of nodes of the ${}^3\text{He}$ radial wave functions increases, the corresponding probability densities $|R_{nl}(r)|^2$ drift towards smaller rms radii; in particular, we find that while $|R_{1s}(r)|^2$ remains centered at distances slightly larger than the rms radius of the cluster, at least for the values of N_4 here considered, the $3s$ wave functions penetrate the drop if N_4 is above 200.

Figure 4 is similar to the former for ${}^4\text{He}$ drops doped with SF_6 , but only the energies of s states are shown, since the energies of the lowest lying l levels rapidly become degenerate as the ${}^4\text{He}$ drop grows above a few tens of particles. In this case we appreciate that the distortion of the SP potential provided by the external field associated to the molecular impurity is important for the smallest drops, namely, for N_4 below 300. This behavior was observed in Ref. 31 in connection with the systematics of pure and doped ${}^4\text{He}$ clusters; for the sake of additional comparison, the $1s$ energy of the ${}^3\text{He}$ atom in the pure droplets is displayed in dashed lines, showing that ε_{1s} is insensitive to the presence of the SF_6 molecule for these large values of N_4 . In this case, we observe that in the same range of drop sizes, the molecular field strongly binds the ${}^3\text{He}$ atom and at the same time, it lowers

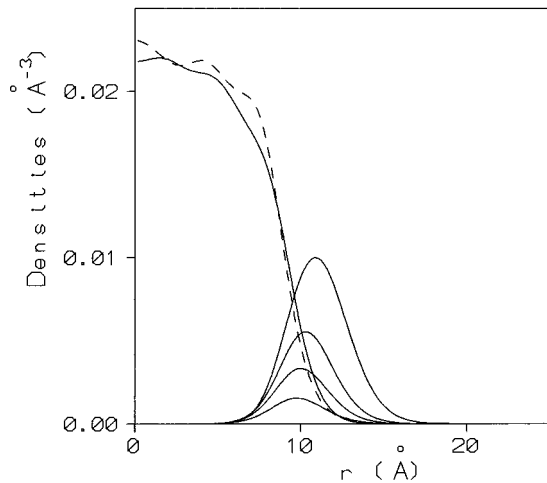


FIG. 7. The densities $\rho_4(r)$ (\AA^{-3}) of the $^4\text{He}_{70}$ drop for $N_3=8$ (full line) and 72 (dashed line), and $\rho_3(r)$ (\AA^{-3}) for $N_3=8, 18, 32,$ and 72 from bottom to top, as functions of r (\AA).

and compresses the whole spectrum to a significant amount. The effect of the SF_6 potential on the ^3He systematics disappears for N_4 above 300, due to the fact that at the distances where the wave functions $\phi_j(\vec{r})$ concentrate, the molecular potential is almost vanishing. The source for the ^3He potential is the density $\rho_4(\vec{r})$, which at these radii is also rather insensitive to the presence of the impurity.

In Fig. 5 we show the radial probability density $|R_{1s}(r)|^2$, as a function of the distance to the center of the droplet for different N_4 . Figure 6 displays the same quantity for the corresponding doped drops. A comparison of these two pictures indicates that for the smaller drop sizes the foreign molecule not only prevents the ^3He atom from reaching the central region, but compresses the whole pattern. For every N_4 , the ^3He atom is pushed towards smaller radii; we can also observe that for the $^4\text{He}_{70}$ drop, two peaks have developed and the outer one becomes the most important as the drop size keeps growing. For $N_4=112$ the peak lies slightly

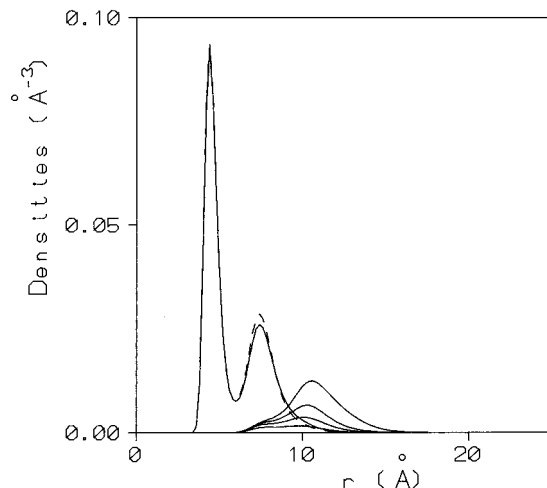


FIG. 8. The densities $\rho_4(r)$ (\AA^{-3}) of the $^4\text{He}_{70} + \text{SF}_6$ drop for $N_3=8$ (full line) and 72 (dashed line), and $\rho_3(r)$ (\AA^{-3}) for $N_3=8, 18, 32,$ and 72 from bottom to top, as functions of r (\AA).

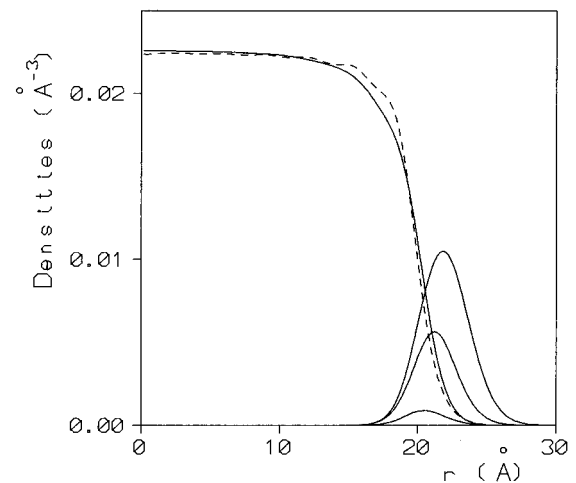


FIG. 9. The densities $\rho_4(r)$ (\AA^{-3}) of the $^4\text{He}_{728}$ drop for $N_3=18$ (full line) and 288 (dashed line), and $\rho_3(r)$ (\AA^{-3}) for $N_3=18, 128,$ and 288 from bottom to top, as functions of r (\AA).

to the left of the corresponding one in the pure cluster, whose height it moderately exceeds, remaining more concentrated. For N_4 larger than 300, the probability densities are very similar, indicating that the presence of the molecular impurity has little influence on the ^3He surface states (Andreev states). It is worthwhile noticing that the accuracy of this type of calculations has been recently found comparable³¹ to that of variational descriptions of small clusters of liquid ^4He .⁹

IV. THE CASE OF PURE AND DOPED ^4He DROPLETS WITH VARIABLE NUMBER OF ^3He ATOMS

As a case of study, in this section we shall concentrate our analysis on two ^4He clusters of rather different size, namely, $N_4=70$ and 728. In Fig. 7 we show the densities $\rho_4(r)$ and $\rho_3(r)$ for different N_3 values between 8 and 72, as functions of the radial distance, for the $^4\text{He}_{70}$ drop. The number of

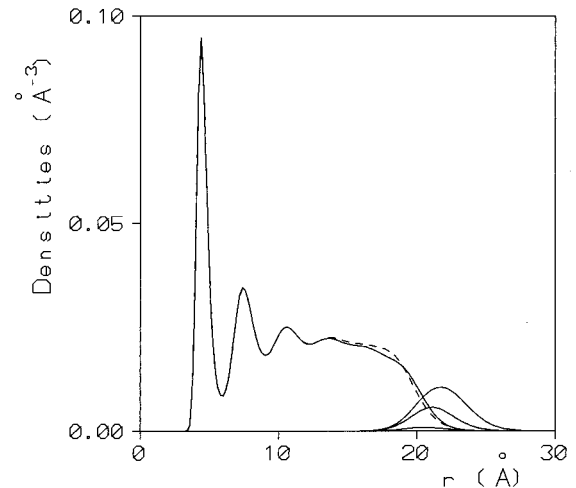


FIG. 10. The densities $\rho_4(r)$ (\AA^{-3}) of the $^4\text{He}_{728} + \text{SF}_6$ drop for $N_3=18$ (full line) and 288 (dashed line), and $\rho_3(r)$ (\AA^{-3}) for $N_3=18, 128,$ and 288, from bottom to top, as functions of r (\AA).

TABLE II. Energetics of mixed drops. $N_4=70$ pure (columns 2–4) and doped with SF_6 (columns 5–7).

N_3	$E/(N_3+N_4)$ (K)	μ_4 (K)	μ_3 (K)	$E/(N_3+N_4)$ (K)	μ_4 (K)	μ_3 (K)
0	-2.97	-4.17		-12.95	-5.46	
8	-3.06	-4.35	-2.68	-12.72	-5.38	-3.28
18	-3.00	-4.45	-2.59	-11.62	-5.39	-3.13
32	-2.92	-4.60	-2.47	-10.42	-5.49	-2.96
50	-2.81	-4.80	-2.29	-9.25	-5.63	-2.68
72	-2.68	-5.05	-2.08	-8.16	-5.80	-2.31

^3He atoms has been chosen so as to fill a shell of their single-particle spectrum. Figure 8 shows the same magnitudes for the cluster $^4\text{He}_{70} + \text{SF}_6$. We may notice in these two pictures a slight tendency of $\rho_3(r)$ to penetrate more deeply into the pure host cluster. It should be remarked that whatever the value of N_3 , the density ρ_3 remains peaked at the surface of the $^4\text{He}_{70}$ drop; we can observe as well a slight inward compression of this surface as the ^3He bubble grows larger. In Fig. 8, an inner peak in ρ_3 that insinuates for high N_3 may indicate the attraction of the low ^4He density in the dip of the drop profile, intending to build a new ‘‘Andreev-like’’ state. Up to the largest N_3 value we have considered for this cluster, namely, 72, we have not found any evidence of the ^3He atoms diluting in the bulk of the drop.

Figures 9 and 10 are the same as Figs. 7 and 8 for $N_4=728$. It is clear that in any configuration, the density $\rho_3(r)$ definitely sits at the surface of the drop even for the largest configuration we have studied. It is also clear that the larger the hosting ^4He drop, the larger its surface and consequently, the higher the number of ^3He atoms it may accommodate. The above mentioned compressional effect induced by the latter on the bosonic cluster is also present.

Concerning the energy systematics of these systems, the major characteristics we report are that increasing amounts of ^3He atoms introduce important attractive contributions into the chemical potential of the ^4He atoms, and repulsive ones in the chemical potential of ^3He atoms. Also, the drops become less bound as we increase N_3 at fixed N_4 . This is due to the energy per particle difference between liquid ^3He and

^4He , -2.49 and -7.15 K, respectively. These facts can be visualized in Table II, where we show the total energy per particle and the chemical potentials of ^4He and ^3He for pure and doped $^4\text{He}_{70}$ clusters as functions of N_3 . Table III contains the same quantities for $^4\text{He}_{728}$ drops. Observing these behaviors we realize that the presence of an impurity modifies the energetics to an important amount in the cluster $N_4=70$, providing stronger binding in all the cases here shown; this effect, however, becomes less significant for larger number of ^4He atoms.

V. SUMMARY

In this work we have performed a detailed study of the energetics and structure of mixed ^3He - ^4He clusters, either pure or doped with a SF_6 molecule. For this sake, we have used a new density functional that improves previous descriptions of liquid helium mixtures and that through the explicit incorporation of finite-range interaction terms, provides a good adjustment of the surface tensions of the ^3He and ^4He free surfaces and of the ^3He - ^4He liquid interface. We have considered, on the one hand, the type of spectrum and ground-state wave functions that a pure or a doped ^4He drop furnishes to one ^3He atom, and on the other, the density configurations of pure and doped clusters with various numbers of atoms of each class, N_3 and N_4 .

In accordance with Refs. 20 and 21 the present investigation shows that a single ^3He atom immersed into a ^4He cluster has a SP spectrum whose lowest energy state smoothly approaches the Andreev state in the liquid-free surface; in this context, adding the molecular impurity modifies the structure and the energetics of these SP states only for the smallest numbers N_4 . Increasing the number of ^3He atoms gives rise to interesting structural features, one of which is that ^3He atoms locate on the surface of the ^4He cluster regardless the particular combination (N_3, N_4) , at least up to a few hundreds of atoms of either class. Taking into account that the structure of liquid mixtures, for concentrations above the maximum solubility of ^3He in ^4He , corresponds to an homogeneous ^3He - ^4He solution plus a segregated phase consisting of pure ^3He , it is apparent from the present calculations that much larger amounts of atoms are needed to visualize the onset of ^3He dilution.

As a final remark, we would like to stress the fact that recently, large ^3He drops containing a small fraction of ^4He atoms and doped with sulfur hexafluoride have been produced and mass analyzed.¹² Experimental data and determination of the rotational constants for the SF_6 spectra indicate

TABLE III. Energetics of mixed drops. $N_4=728$ pure (columns 2–4) and doped with SF_6 (columns 5–7).

N_3	$E/(N_3+N_4)$ (K)	μ_4 (K)	μ_3 (K)	$E/(N_3+N_4)$ (K)	μ_4 (K)	μ_3 (K)
0	-5.16	-5.80		-6.30	-5.80	
18	-5.14	-5.80	-3.86	-6.24	-5.81	-3.87
128	-4.94	-5.89	-3.40	-5.90	-5.89	-3.40
288	-4.63	-6.08	-2.71	-5.44	-6.08	-2.70

that ^4He particles build up a first atom shell around the foreign molecule, in agreement with the present theoretical results.

ACKNOWLEDGMENTS

It is a pleasure to thank Professor J.P. Toennies and Dr. A. Vilesov for useful correspondence. This work has been

performed under Grants Nos. EX071/95 from University of Buenos Aires, Argentina, PB95-1249 and PB92-0820 from CICYT, Spain, and Program GRQ94-1022 from Generalitat of Catalunya. One of us (E.S.H.) is grateful to the Department d'Estructura i Constituents de la Matèria (Universitat de Barcelona) for warm hospitality and support during various stays.

-
- ¹J.P. Toennies, in *The Chemical Physics of Atomic and Molecular Clusters*, Proceedings of the International School of Physics "Enrico Fermi," Course CVII, Varenna, 1988 (North-Holland, Amsterdam, 1990), p. 597.
- ²K.B. Whaley, *Int. Rev. Phys. Chem.* **13**, 41 (1994).
- ³M. Lewerenz, B. Schilling, and J.P. Toennies, *Chem. Phys. Lett.* **206**, 381 (1993).
- ⁴W. Schoellkopf and J.P. Toennies, *Science* **256**, 1345 (1994).
- ⁵S. Goyal, D. L. Schutt and G. Scoles, *J. Phys. Chem.* **97**, 2236 (1993).
- ⁶M. Hartmann, R. B. Miller, J. P. Toennies, and A. Vilesov, *Phys. Rev. Lett.* **75**, 1566 (1995).
- ⁷S. A. Chin and E. Krotscheck, *Phys. Rev. B* **52**, 10 405 (1995).
- ⁸E. S. Hernández and M. Barranco, *Phys. Rev. B* **51**, 9364 (1995).
- ⁹M. A. McMahon, R. N. Barnett, and K. B. Whaley, *J. Chem. Phys.* **104**, 5080 (1996).
- ¹⁰F. Dalfovo, *Z. Phys. D* **29**, 61 (1994).
- ¹¹G. De Toffol, F. Ancilotto, and F. Toigo, *J. Low Temp. Phys.* **102**, 381 (1996).
- ¹²J. Harms, M. Hartmann, J.P. Toennies, and A.F. Vilesov, *J. Mol. Spectrosc.* (to be published).
- ¹³A. Guirao, M. Pi and M. Barranco, *Z. Phys. D* **21**, 185 (1991).
- ¹⁴V.R. Pandharipande, S.C. Pieper, and R. B. Wiringa, *Phys. Rev. B* **34**, 4571 (1986).
- ¹⁵S. Stringari and J. Treiner, *J. Chem. Phys.* **87**, 5021 (1987).
- ¹⁶S. Weisgerber and P.-G. Reinhard, *Z. Phys. D* **23**, 275 (1992).
- ¹⁷M. Barranco, D. M. Jezek, E. S. Hernández, J. Navarro, and Ll. Serra, *Z. Phys. D* **28**, 257 (1993).
- ¹⁸Ll. Serra, J. Navarro, M. Barranco, and Nguyen Van Giai, *Phys. Rev. Lett.* **67**, 2311 (1991).
- ¹⁹M. Barranco, J. Navarro, and A. Poves, *Phys. Rev. Lett.* **78**, 4729 (1997).
- ²⁰F. Dalfovo, *Z. Phys. D* **14**, 263 (1989).
- ²¹A. Belić, F. Dalfovo, S. Fantoni, and S. Stringari, *Phys. Rev. B* **49**, 15 253 (1994).
- ²²F. Dalfovo, A. Lastrì, L. Pricauptenko, S. Stringari, and J. Treiner, *Phys. Rev. B* **52**, 1193 (1995).
- ²³F. Dalfovo, Ph.D. thesis, University of Trento, 1989.
- ²⁴N. Pavloff and J. Treiner, *J. Low Temp. Phys.* **83**, 15 (1991).
- ²⁵H. C. Chocolats, R. M. Mueller, J. R. Owers-Bradley, Ch. Buchal, M. Kubota, and F. Pobell, in *Low Temperature Physics LT17*, edited by U. Eckern, A. Schmid, W. Weber and H. Wuhl (Elsevier, New York, 1984).
- ²⁶M. Casas, F. Dalfovo, A. Lastrì, Ll Serra, and S. Stringari, *Z. Phys. D* **35**, 67 (1995).
- ²⁷D. Vautherin and D. M. Brink, *Phys. Rev. C* **5**, 626 (1972).
- ²⁸R. T. Pack, E. Piper, G. A. Pfeffer, and J. P. Toennies, *J. Chem. Phys.* **80**, 4940 (1984).
- ²⁹Finite range density functionals yield density profiles having narrower surfaces than local density functionals. This is the reason why we find a better agreement with experiment than Ref. 20, see Ref. 21.
- ³⁰D.O. Edwards and W.F. Saam, *Progress in Low Temperature Physics*, edited by D.F. Brewer (North Holland, Amsterdam, 1978), Vol. II A, p. 283.
- ³¹S. M. Gatica, E. S. Hernández, and M. Barranco, *J. Chem. Phys.* **107**, 927 (1997).
- ³²C. Ebner and D. O. Edwards, *Phys. Rep.* **2**, 77 (1970).
- ³³L.S. Balfour, Ph.D. thesis, Haifa, 1978.